ACS APPLIED MATERIALS & INTERFACES

Research Article

www.acsami.org

High Energy Density Aqueous Electrochemical Capacitors with a KI-KOH Electrolyte

Xingfeng Wang,[†,⊥] Raghu S. Chandrabose,[†,⊥] Sang-Eun Chun,[‡] Tianqi Zhang,[†] Brian Evanko,[§] Zelang Jian,[†] Shannon W. Boettcher,[‡] Galen D. Stucky,[§,∥] and Xiulei Ji*[,†]

[†]Department of Chemistry, Oregon State University, Corvallis, Oregon 97331, United States

[‡]Department of Chemistry and Biochemistry, University of Oregon, Eugene, Oregon 97403, United States

[§]Materials Department, and [∥]Department of Chemistry and Biochemistry, University of California, Santa Barbara, California 93106, United States

Supporting Information

ABSTRACT: We report a new electrochemical capacitor with an aqueous KI-KOH electrolyte that exhibits a higher specific energy and power than the state-of-the-art nonaqueous electrochemical capacitors. In addition to electrical double layer capacitance, redox reactions in this device contribute to charge storage at both positive and negative electrodes via a catholyte of IO_x^-/I^- couple and a redox couple of H_2O/H_{ad}, respectively. Here, we, for the first time, report utilizing IO_x^-/I^- redox couple for the positive electrode, which pins the positive electrode potential to be 0.4−0.5 V vs Ag/AgCl. With the positive electrode potential pinned, we can polarize the cell to 1.6 V without breaking down the aqueous electrolyte so that the negative electrode potential could reach −1.1 V vs Ag/AgCl in the basic electrolyte, greatly enhancing energy storage. Both mass spectroscopy and Raman spectrometry confirm the formation of IO_3^- ions (+5) from I^- (−1) after charging. Based on the total mass of electrodes and electrolyte in a practically relevant cell configuration, the device exhibits a maximum specific energy of 7.1 Wh/kg, operates between −20 and 50 °C, provides a maximum specific power of 6222 W/kg, and has a stable cycling life with 93% retention of the peak specific energy after 14 000 cycles.

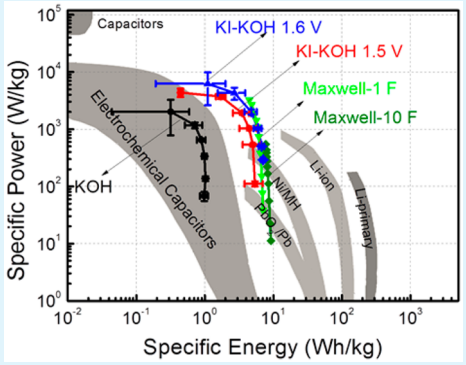

KEYWORDS: *aqueous electrochemical capacitor, redox electrolyte, KI and KOH mixture, iodate, high energy, high power*

INTRODUCTION

Electrochemical capacitors (ECs) have a broad range of applications.[1−3] ECs store energy by two mechanisms: electrical double layer (EDL) capacitance and pseudocapacitance.[4] EDL capacitors (EDLCs) employ electrodes comprising activated carbons (ACs) with high specific surface areas. The capacitance derives from electrostatic interaction between the polarized electrode surface and the attracted solvated ions, thus forming an EDL on each electrode. EDLCs exhibit excellent cycling life and high specific power but limited energy density.[5,6] To date, much effort has been devoted to the syntheses of nanoporous carbons with tunable properties,[7] to understanding the interaction between solvated ions and the electrode surface, and to elucidating the mechanisms of EDL formation.[5,8−17] Pseudocapacitors, on the other hand, are essentially high-rate batteries employing redox active electrodes that can operate on either of the two mechanisms: (1) surface/near-surface redox reactions and (2) intercalation redox reactions.[18] Great progress has been made in developing pseudocapacitors based on conductive polymers[19−22] and various transition metal oxides,[23−29] but such chemistries often suffer compromised power and cycle life compared to EDLCs.

Recently, integrating solvated redox-active species into electrolytes has emerged as a new strategy to increase the energy density of EDLCs.[30−33] The principle behind this strategy is that the redox species remain solvated during cycling, providing faster diffusion and kinetics than solid-state materials. As Lota et al. reported, KI-solvated aqueous electrolyte with I_3^-/I^- redox couple displays an enhanced capacitance due to the electrochemical behavior of carbon/iodide interface.[34,35] It was also published that ECs with KI as an additive to an electrolyte of sulfuric acid exhibit enhanced specific energy.[36] In an alkaline poly(vinyl alcohol) gel electrolyte, KI was also added to increase the ionic conductivity and pseudocapacitance.[37]

Along this line, we reported a hybrid electrochemical battery−supercapacitor system utilizing an electrolyte containing anionic catholyte and cationic anolyte derived from the mixture of solvated KI and $VOSO_4$, which showed improved energy density and good cyclability.[38] Very recently, a combined electrolyte with two physically separated compart-

Received: May 28, 2015
Accepted: August 27, 2015
Published: August 27, 2015

ACS Publications © 2015 American Chemical Society

DOI: 10.1021/acsami.5b04677
ACS Appl. Mater. Interfaces 2015, 7, 19978−19985

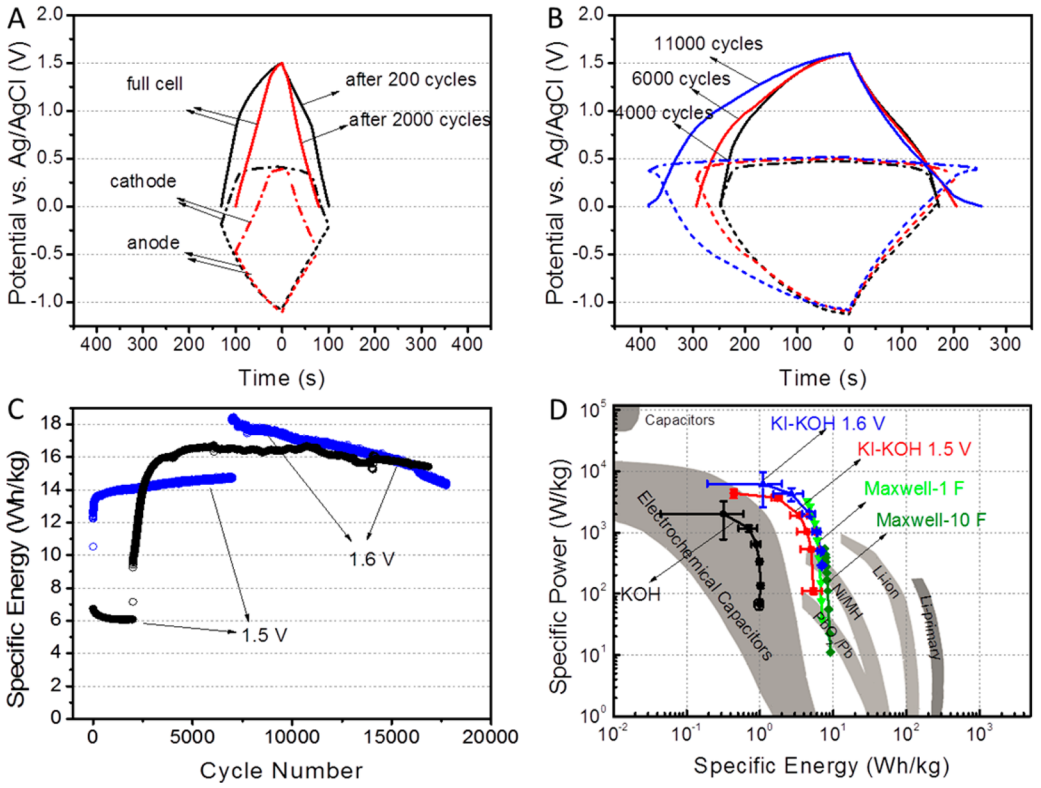

Figure 1. Three electrode galvanostatic charge−discharge at 1 A/g (A) when charging to 1.5 V and (B) when charging to 1.6 V. (C) Long-term cycling at 5 A/g (black in Swagelok cell, blue in coin cell, specific energy calculated based on the mass of both electrodes). (D) Ragone plot calculated based on the total mass of both electrodes and electrolyte.[40] Adapted by permission from Macmillan Publishers Ltd.: [Nature Materials] (ref 40), copyright (2008).

ments: pH-neutral KI for the positive electrode side and KOH for the negative electrode side was reported.[39] In this cell, the maximum cell voltage reaches 1.5 V, compared to 1.0 V typically reported by other aqueous-based ECs. The voltage of 1.5 V for the cell is achieved for polarizing the negative electrode to −1.4 V vs standard hydrogen electrode (SHE) and the positive electrode to 0.1 V vs SHE. In this cell, the positive electrode operates on the I_3^-/I^- redox couple, which pins the positive electrode at 0.1 V vs SHE. It appears that the hydrogen evolution reaction is suppressed even down to −1.4 V vs SHE, which allows, in this paper, an investigation on hydrogen adsorption/desorption redox reactions on the surface of porous carbon.

Herein, we, for the first time, report the electrochemical properties of an aqueous electrolyte of mixed KI and KOH. The motivation of mixing KI and KOH is to explore the possibility of using the redox couple of IO_x^-/I^-, where the IO_x^- can be either IO_3^- or IO_4^-, which is confirmed by mass spectroscopy and Raman spectrometry. This is because, according to the Pourbaix diagram of iodine, when the cell is polarized, the I^- ions in a basic electrolyte will be oxidized into IO_x^-, that is, IO_3^- and/or IO_4^-, instead of I_3^-, pinning the potential on the positive electrode side. Therefore, the full cell voltage can be high as long as the hydrogen evolution reaction is effectively suppressed by the basic electrolyte on the negative electrode as well as a high overpotential. With this KI/KOH electrolyte, here the reported aqueous cell approaches a voltage of 1.6 V.

EXPERIMENTAL SECTION

Preparation of Carbon Electrodes. Carbon fibers (Donacarbo S-241 from Osaka gas Co., Ltd.) were activated to obtain a high specific surface area under CO_2 with a gas flow rate of 229 cc/min at 920 °C for 18 h. Such conditions are the result of optimization to obtain a surface area above 2400 m^2/g. In forming an electrode, the obtained activated carbon was mixed in amyl acetate with polytetrafluoroethylene (PTFE) and carbon black (Super P) by a weight ratio of 8/1/1. After drying in air, the mixture was processed into a self-standing film by a rolling machine, which was later dried inside a vacuum oven at 80 °C overnight. The active mass for the final electrodes is ∼5.1 mg/cm^2, where the electrode is of a thickness of ∼90 μm.

Porosity Measurements of Porous Carbon. Specific surface area was measured by using a Micrometrics TriStar II 3020 analyzer. Samples were degassed under N_2 at 250 °C for 4 h before the measurements. BET surface area and pore size distribution were obtained and calculated from N_2 sorption isotherms at −196 °C.

Electrochemical Characterization. Three-electrode cells were assembled in custom-made T-Swagelok cells, consisting of two identical carbon electrodes and a saturated Ag/AgCl electrode as the reference electrode (RE). The three-electrode cell in this work is slightly different from the conventional configuration of three-electrode cells, where there typically is a working electrode, a counter electrode, that is, a platinum wire, and a reference electrode. In our system, two identical carbon electrodes serve as both working and counter electrodes. Coin cells were made in a symmetric configuration, using a polycarbonate membrane as the separator with a thickness of 9 μm and porosity of 17.7% (Sterlitech Corporation). Each coin cell contains only 10 μL of electrolyte to test the performance with limited electrolyte, which is sufficient to fill up the porosity of both electrodes and the separator. By calculation, the void volume inside both electrodes and separator is only ∼8.40 μL (see Supporting Information for detailed calculation). The galvanostatic charge−discharge tests were conducted on a Maccor Series 4000. The cyclic voltammetry

DOI: 10.1021/acsami.5b04677
ACS Appl. Mater. Interfaces 2015, 7, 19978−19985

(CV) measurements were carried out on an EC-lab VMP3 instrument. Specific capacitance C (F/g) was calculated from galvanostatic charge−discharge measurements with the equation:

$$C = \frac{2It}{mV} \quad \text{(A)}$$

where I is the constant current (mA), t is the discharge time (s), m is the active mass on one electrode (mg), and V is the maximum cell voltage (V). Specific capacitance can be also obtained from CV measurements with the equation:

$$C = \frac{1000}{mv(V_c - V_a)} \int_{V_c}^{V_a} I(V)\, dV \quad \text{(B)}$$

where m is the active mass on one electrode (mg), v is the scan rate (mV/s), V_c is the cathodic potential (V), V_a is the anodic potential (V), and I is the current response (mA).

Specific energy E (Wh/kg) was calculated by integrating the area beneath the discharge curves with the equation:

$$E = \frac{1000I}{3600m} \int_t^0 V(t)\, dt \quad \text{(C)}$$

where I is the discharge current (mA), m is the total mass of both electrodes and electrolyte (mg), t is the discharge time (s), and V is the cell voltage (V).

Average specific power P (W/kg) was calculated from the following equation,

$$P = \frac{3600E}{t} \quad \text{(D)}$$

where t is the discharge time (s), and E is the specific energy (Wh/kg).

Nonaqueous Maxwell capacitors (BCAP0001-1F and BCAP0010-10F) were tested at different current densities for comparison. We count only the mass of electrodes and electrolyte for these commercial cells for comparison purposes.

Mass Spectrometry (MS). The cell was cycled for 3000 cycles at a voltage of 1.5 V before it was taken apart to collect the charged electrolyte. Electrolyte was diluted by 1000 times before tests. A Waters Synapt G1 HDMS mass spectrometer equipped with a Z-spray electrospray ionization source was used to acquire the MS data in the negative-ion mode. The voltages of capillary, sampling cone, and extraction cone are 1300, 40, and 4.0 V respectively. The source and desolvation temperatures are 80 and 450 °C.

Raman Spectroscopy. Raman spectra were measured in DXR SmartRaman with 780 nm laser as the excitation source. Through the 50-μm slit, data were collected in 8 exposures with 8 s each time.

RESULTS AND DISCUSSION

After CO_2 activation of carbon fibers, a high surface area of 2405 m^2/g and a total pore volume of 1.0 cc/g were obtained (Figure S1). With the nanoporous activated carbon as the electrodes, we assembled three-electrode cells and two-electrode symmetric cells to investigate the electrochemical behavior of an aqueous electrolyte comprising 4 M KI and 1 M KOH (Figure S2). Galvanostatic charge−discharge cycles were collected in a three-electrode cell at a current density of 1 A/g, which is normalized to carbon mass in one electrode. Figure 1A shows the potential profiles when the three-electrode cell is charged to 1.5 V. At the 200th cycle, full cell potential profiles exhibit sectioned sloping regions, while a well-defined plateau at 0.4 V vs Ag/AgCl is observed at the positive electrode, which is from the redox reactions involving iodide. This is consistent with the Pourbaix diagram, which shows the predominant oxidized species in basic aqueous media as iodates, IO_3^-. On the negative electrode, the potential profiles are slightly curved lines, indicating some faradaic reactions in parallel with the capacitive charging on the activated carbon.

From the 200th cycle to the 2000th cycle, specific energy faded. At the 2000th cycle, we conducted the three-electrode charge−discharge test (red curves in Figure 1A). Interestingly, the potential plateau on the positive electrode was diminished compared to the profile at the 200th cycle. We also observed that the potential of short circuit (PSC) of carbon electrodes was significantly lowered from −0.2 to −0.5 V vs a Ag/AgCl reference electrode after 1800 cycles. The negative shift of PSC caused less capacitive contribution to total charge storage on the negative electrode, and more capacitive contribution on the positive electrode. Because the combination of faradaic and capacitive charge storage on the positive electrode must equal the capacitive charge storage (this may include hydrogen adsorption) on the negative electrode, when the PSC shifts negatively, less charge-storage from the redox reactions is needed on the positive electrode at the same cell polarization of 1.5 V.

After the 2000th cycle, we increased the cell voltage from 1.5 to 1.6 V in order to better take advantage of the redox reactions on the positive electrode. As shown in Figure 1C, the specific energy based on the mass of both electrodes increased from 6 to 16 Wh/kg (the electrolyte mass was not included due to the excessive electrolyte in three-electrode cell). We collected three-electrode charge−discharge potential profiles at the 4000th, 6000th and 11 000th cycles, as shown in Figure 1B. The negative electrode polarization was observed to be −1.1 V vs Ag/AgCl, consistently. The positive electrode polarization increased from 0.4 to 0.5 V, showing a large plateau, which resulted in a dramatic increase in specific energy. However, upon increasing the cell voltage from 1.5 to 1.6 V, the Coulombic efficiency decreases. In the 1999th cycle, the Coulombic efficiency is 96.8%, which decreases to 86.9% in the 2001st cycle. We attribute the lowered Coulombic efficiency to the irreversible reactions on the negative electrode side. As revealed in Figure 1B, it is evident that the potential profiles are highly reversible on the positive electrode in the 4000th, 6000th, and 11 000th cycles. However, on the negative electrode side, plateaus are observed near −1.0 V vs Ag/AgCl during charging, whereas such plateaus are absent in the following discharge, resulting in the lowered Coulombic efficiency and energy efficiency. For the irreversible reaction on the negative electrode, we attribute it to a certain extent of hydrogen evolution reaction (HER), where the evolved hydrogen gas may not be oxidized reversibly. From the 4000th cycle to 11 000th cycle, the consistency of cell potential profiles is responsible for the stable cycling performance, as shown in Figure 1C. From the 3000th cycle to 17 000th cycle, the fading in specific energy was only 7%, indicating excellent reversibility of the KI-KOH system. Coin cells were also tested, which is shown in blue in Figure 1C. The specific energy faded from 18 to 14 Wh/kg from the 7000th to the 17 000th cycle. Further cell optimization will likely enable these already impressive values to be improved.

The fact that PSC shifts to lower values during the initial cycling at cell polarization of 1.5 V but increases over further cycling at cell polarization of 1.6 V is very interesting. However, a comprehensive investigation of PZC and PSC of the electrodes by itself can be an independent project, which is thus beyond the scope of this work. Here, we provide our thoughts on this issue supported by experimental evidence.

The lowered PSC during the initial cycling at a cell polarization of 1.5 V can be related to the hydrogen adsorption on the negative electrode. When some irreversibly adsorbed

DOI: 10.1021/acsami.5b04677
ACS Appl. Mater. Interfaces 2015, 7, 19978−19985

hydrogen atoms cover the negative electrode, its PZC decreases as documented by prior studies,[41,42] which may lower the PSC for the cell. Interestingly enough, upon increasing the cell polarization to 1.6 V, the surface of carbon positive electrode was, indeed, oxidized to a certain extent, where, revealed by energy dispersive X-ray (EDX) spectroscopy, the mass ratio of oxygen over carbon of the positive electrode increases from 2.8% to 5.7% after cycling for 2000 cycles (Figure S3). It is known that oxidized carbon surface causes an increased PZC of porous carbon electrode,[41,42] which overcomes to the impact from the negative electrode and causes the PSC to increase over cycling at 1.6 V.

Another issue is whether applying 1.6 V to the cells causes breaking down of the aqueous electrolyte. We recognize that the thermodynamic potential value of water oxidation is lower than the potential where the positive electrode is finally polarized at the end of charging process. However, such oxidation reaction is normally kinetically inhibited even if catalysts are employed. Oxidizing water, that is, via the oxygen evolution reaction (OER), is no trivial task due to the large overpotential. Even with noble metal oxides as catalysts, for example, rutile-type RuO_2, the state-of-the-art catalyst for OER, the reaction still suffers overpotential of 0.2 V.[43] As indirect evidence that OER is not severe, the cells with very limited volume of electrolyte, that is, 10 μL, can be run for well more than 15 000 cycles. The electrolyte would be soon consumed if OER or hydrogen evolution reaction (HER) occurred to a significant extent, which is clearly not the case.

A Ragone plot is a straightforward way to show specific energy and power, which we calculated based on the combined mass of both carbon electrodes and electrolyte. Cells with an electrolyte of 4 M KI and 1 M KOH, polarized to either 1.5 or 1.6 V were tested at 3, 5, 10, 20, 50, and 100 A/g, respectively (Figure 1D). To compare our system with aqueous EDLCs, cells with an aqueous electrolyte of 6 M KOH polarized to 1 V were also tested. Cells with the KI/KOH electrolyte exhibit superior performance in both specific energy and power, compared to the KOH-based EDLC. At 3 A/g and charged to 1.6 V, the KI-KOH cell obtained 7.1 Wh/kg and 291 W/kg, while at 100 A/g, the cell exhibits 1.1 Wh/kg and an impressive power of 6221 W/kg, which is comparable with the state-of-the-art EDLCs based on nonaqueous electrolytes (2 types from Maxwell) (Figure 1D). Additionally, our system uses a cost-effective and safe aqueous electrolyte, which is encouraging for potential practical applications.

We next tried to understand the enhanced performance of the KI/KOH electrolyte. Referring to the iodine Pourbaix diagram (Figure S4), the possible species that exist at pH 14 are I^-, IO_3^-, and $H_2IO_6^{3-}$. When I^- is oxidized during charging, the final species could be either IO_3^- or $H_2IO_6^{3-}$, corresponding to 6 or 8 total electrons transferred.

The mechanism of IO_3^- formation from I_2 has been reported and discussed in literature.[44,45]

$$I_2 + H_2O \rightarrow I^- + HOI + H^+ \quad (1)$$

$$3HOI \rightarrow IO_3^- + 2I^- + 3H^+ \quad (2)$$

In the KI/KOH electrolyte, I^- is oxidized to I_2 first that disproportionates, in a basic solution, to form hypoiodous acid (HOI). HOI further disproportionates to form iodate. The overall reaction is as follows:

$$I^- + 6OH^- \rightarrow IO_3^- + 3H_2O + 6e^- \quad (3)$$

In order to identify the I-containing species in the electrolyte, we collected MS for the electrolyte (4 M KI and 1 M KOH) from a two-electrode coin cell after 3000 cycles as well as a standard sample of KIO_3 solution (Figure 2). For the charged

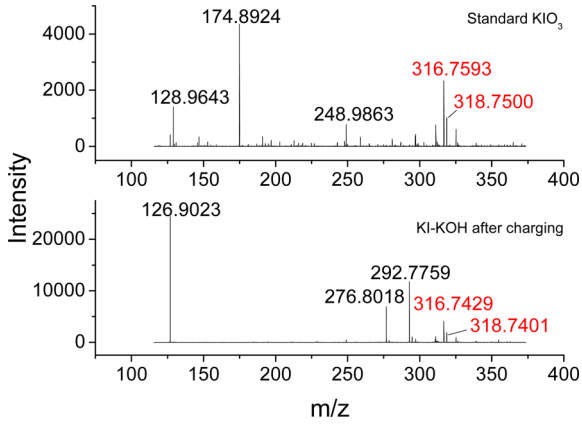

Figure 2. Mass spectra of a standard KIO_3 solution and the electrolyte of KI-KOH after cycling ending when fully charged.

KI+KOH electrolyte, the first three major peaks at 126.9023, 292.7759, and 276.8018 m/z are assigned to be I^- (126.9045 m/z), KI_2^- (292.9074 m/z), and NaI_2^- (276.7987 m/z), respectively. The other two major peaks at 316.7428 and 318.7401 m/z in the charged electrolyte match the peaks at 316.7593 and 318.7500 m/z in the standard KIO_3 solution, which are assigned to $IO_3^-{\cdot}8H_2O$ (317.0087 m/z) and $IO_4^-{\cdot}7H_2O$ (319.0246 m/z), respectively. This presents strong evidence for the formation of iodate and periodate over cycling of our device. This is a fundamental difference between our system and the device investigated by Frackowiak et al.[39]

In order to further confirm the formation of iodate, we conducted Raman spectroscopy measurements for the KI +KOH electrolyte before and after charging by using pure KIO_3 and water as control samples (Figure S5). From the Raman results, the charged electrolyte of KI+KOH shows a much-enhanced signal at 800 cm^{-1} as the standard KIO_3 solution, which can be assigned to the nonpolar stretching vibration of IO_3^- (symmetry A_1).[46] Therefore, both MS and Raman results indicate that IO_3^- (+5) has been formed after charging.

On the negative electrode, the curved charge−discharge potential profiles indicate simultaneous redox reactions and capacitive charging. Hydrogen adsorption/desorption could be responsible for this and the mechanism has been explained and discussed in the literature.[47,48] In alkaline solution, water can be reduced through Volmer reaction 4 to form adsorbed hydrides:

$$H_2O + e^- \rightarrow H + OH^- \quad (4)$$

$$C + H \rightarrow CH_{ad} \quad (5)$$

However, due to Heyrovsky reaction 6 and/or Tafel reaction 7, adsorbed hydrides can be discharged to form H_2, which would result in irreversible capacity loss in our device:

$$CH_{ad} + H_2O + e^- \rightarrow H_2 + OH^- + C \quad (6)$$

$$2H \rightarrow H_2 \quad (7)$$

$$CH_{ad} + CH_{ad} \rightarrow H_2 + 2C \quad (8)$$

For hydride formation to provide significant reversible capacity, the activation barrier for the Heyrovsky and Tafel eqs 6 and 7)

DOI: 10.1021/acsami.5b04677
ACS Appl. Mater. Interfaces 2015, 7, 19978−19985

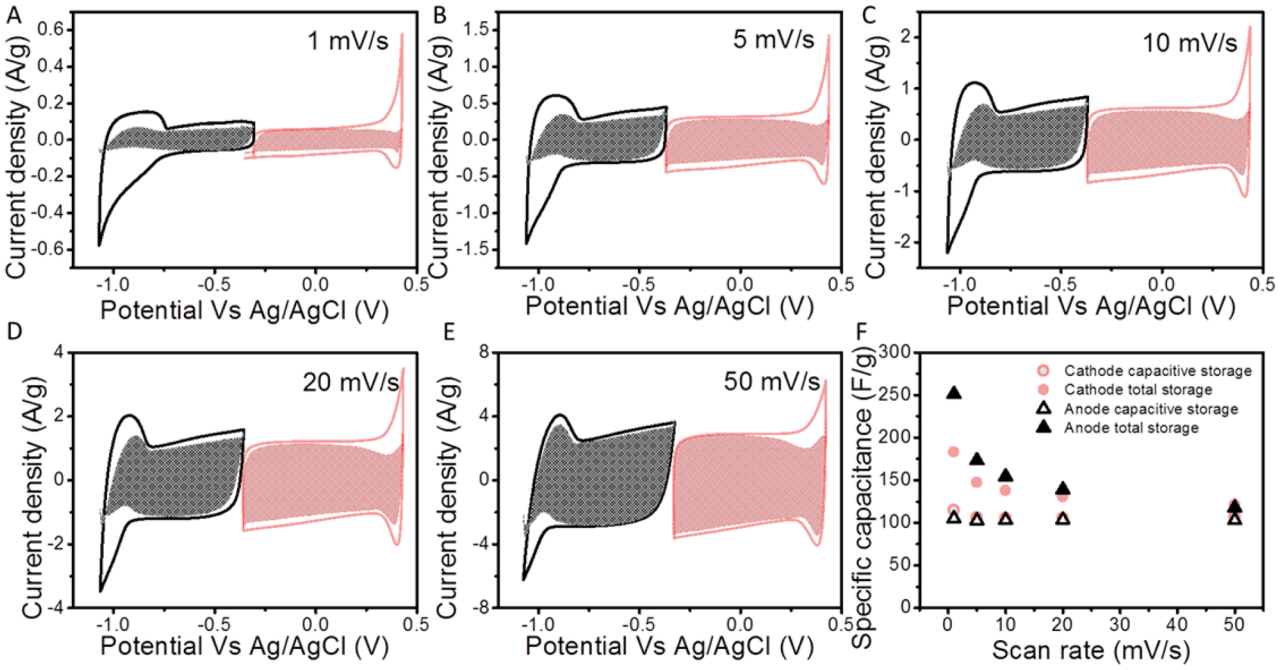

Figure 3. Cyclic voltammetry of three-electrode cell using 4 M KI and 1 M KOH at (A) 1 mV/s, (B) 5 mV/s, (C) 10 mV/s, (D) 20 mV/s, and (E) 50 mV/s. (F) Specific capacitance at different scanning rates: positive electrode in red, and negative electrode in black.

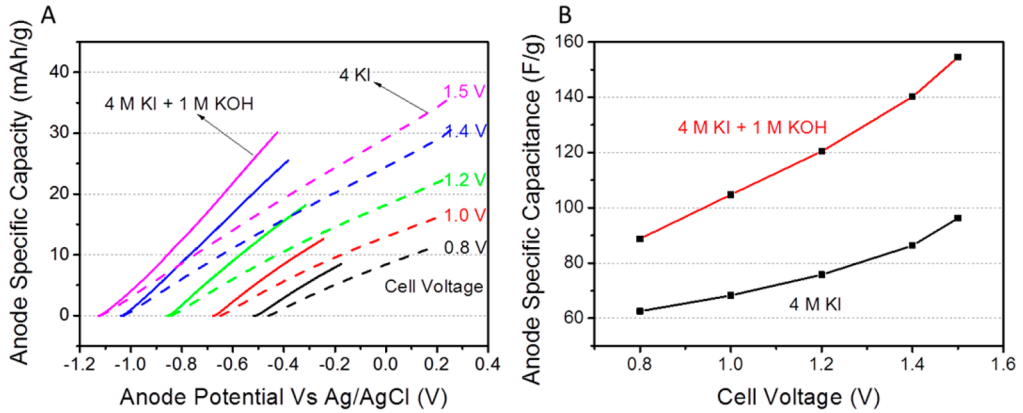

Figure 4. (A) Discharge capacity and (B) capacitance on the negative electrode: Comparison between with and without the presence of KOH.

must be larger than that for the Volmer reaction (eq 4). These conditions are typical in basic media.[39]

Because the charge storage on both positive and negative electrode sides may rely on redox reactions, it is of fundamental interest to evaluate the charge storage mechanisms and compare the contribution from capacitive storage to that from diffusion controlled storage. Thus, CVs were tested in three-electrode cells for both positive and negative electrode at various scanning rates from 1 mV/s to 50 mV/s. From Figure 3, the PSC is about −0.37 V vs Ag/AgCl, and the negative and positive electrode are polarized to −1.06 and 0.44 V, respectively, when the cell is charged to 1.5 V. From −0.7 to 0.3 V, the rectangular shape of CVs indicates the ideal capacitive behavior of the capacitor, while the peaks at −1 and 0.4 V correspond to redox reactions. We attribute the redox peak at −1 V to the hydrogen adsorption and desorption on the porous carbon, which provides a fraction of redox capacitance on the negative electrode, especially at low potential. On the positive electrode, the redox peak at 0.4 V correlates to the redox reaction of iodine-containing species. Inside each CV, the shaded area is the capacitive contribution, that is, current is proportional to scan rate v, which is described as $k_1 v$.[18,49]

The redox reactions are typically diffusion-controlled processes that are proportional to $v^{1/2}$, thus the corresponding current contribution is $k_2 v^{1/2}$. By testing CV at different scanning rates, the coefficients k_1 and k_2 can be calculated for different potentials, and the total current can be deconvoluted into diffusion-controlled and capacitive contributions. As shown in Figure 3, the midpotential region is dominated by capacitive current, and the gap between total current and capacitive current (shaded area) at low potential and high potential is from the diffusion-controlled redox processes, which decreases as the scanning rate increases. We note that diffusion limitations driving the redox reactions likely play a major role in the decrease of current at faster scan rates. In Figure 3F, when the scan rate is increased to 50 mV/s, the total capacitance from negative electrode and positive electrode drops from 251 F/g (1 mV/s) to 118 F/g, and from 183 F/g (1 mV/s) to 122 F/g, respectively. However, little difference is

DOI: 10.1021/acsami.5b04677
ACS Appl. Mater. Interfaces 2015, 7, 19978−19985

observed in the capacitance from the double layer charging process when increasing scanning rates.

In order to further investigate hydrogen adsorption/desorption, galvanostatic charge−discharge profiles at the negative electrode are compared between KI and KI/KOH. In Figure 4A, negative electrode specific capacity (normalized to single electrode mass) is plotted versus negative electrode potential. At higher cell voltage (from 0.8 to 1.5 V), the negative electrode is polarized to more negative values (from −0.5 V to −1.1 V). In the presence of KOH, the slope (capacitance) of the discharge profile is steeper, indicating a stronger capability to store charge. In Figure 4B, higher capacitance is observed using KI/KOH electrolyte, which is attributed to the enhanced hydrogen adsorption/desorption in porous carbon. (More detailed investigation in the Supporting Information.)

Self-discharge is another important factor affecting the capacitor applications. To study the self-discharge, the capacitor was charged to 1.5 V at 1 A/g, and relaxed for 24 h with the open circuit voltage (OCV) recorded. In Figure 5 (green line),

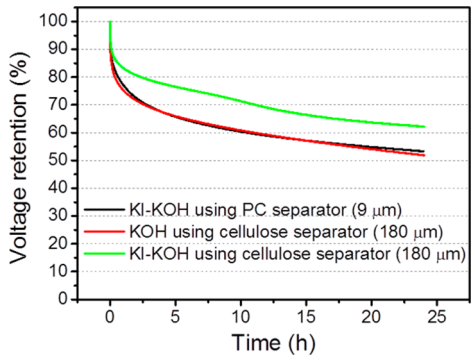

Figure 5. Self-discharge for 24 h with and without of KOH and with separators with different thickness.

for the KI+KOH system, OCV remains at 0.93 V out of 1.5 V (62%) after 24 h. Interestingly, after 24 h, the OCV of the pure EDLC with KOH as the electrolyte was only 0.52 V out of 1 V. We further discovered that the thickness of separator has a significant impact on the rate of self-discharge. When switching the separator with a thickness of 180 μm to the one 9 μm thick, the self-discharge rate turns faster for the KI+KOH system. Yet, with such a thin separator, the rate of KI+KOH is still comparable to the pure KOH system with the separator 180 μm thick. Ongoing studies are focused on understanding the relatively slow self-discharge of the KI/KOH system.

Temperature response is another concern for aqueous capacitors. Therefore, we measured the specific energy based on the combined mass of electrodes and electrolyte and self-discharge from −20 to 50 °C in a constant temperature chamber. Without any additives, the KI+KOH cells can operate at −20 °C due to the freezing point depression. According to Blagden's Law, the theoretical freezing point is calculated to be −23.7 °C, which explains the performance.

Although we use a high concentration of KI, because of its high solubility in water, no effects due to precipitation are found even at −20 °C, so a high capacity is maintained. We observed increasing specific energy and decreasing round-trip energy efficiency as we increased the working temperature (Figure 6A), which can be explained by faster kinetics and diffusion rates at higher temperatures, along with an increased number of side reactions. We also found increasing internal resistance caused by slower ion movement at lower temperatures, but even at −20 °C the IR drop is still below 0.03 V.

Self-discharge could be a problem when we use the cell at temperatures higher than 30 °C, due to increased diffusivity and the resulting self-discharge via a possible redox shuttle mechanism.[50,51] As shown in Figure 6B, after 5 h at open circuit voltage, the OCV dropped to 0.4 V (or lower) at working temperatures above 40 °C. However, when tested at low temperature, self-discharge was slowed down dramatically. Below −10 °C, the cell voltage only dropped to 1.2 V after 5 h.

CONCLUSION

The advanced redox electrolyte of KI-KOH combines two redox energy-storage processes in aqueous electrochemical capacitors: hydrogen adsorption/desorption and IO_3^-/I^- redox reactions. With the presence of KOH, we are able to charge the cell to 1.6 V and achieve a specific energy above 7 Wh/kg (accounting for the mass of both electrodes and electrolyte) and an average specific power above 6200 W/kg. Excellent cyclability is obtained with only 7% loss in device specific energy after 14 000 cycles. For self-discharge, over 62% of the voltage remains after 24 h, slower than traditional EDLC (6 M KOH). The large operating temperature window is practically important. This electrolyte thus constitutes important progress in the development of "redox-enhanced" electrochemical capacitors, as it promises an efficient mechanism to increase the storage of electrical energy with long cycle life and the potential for low cost and safe operation.

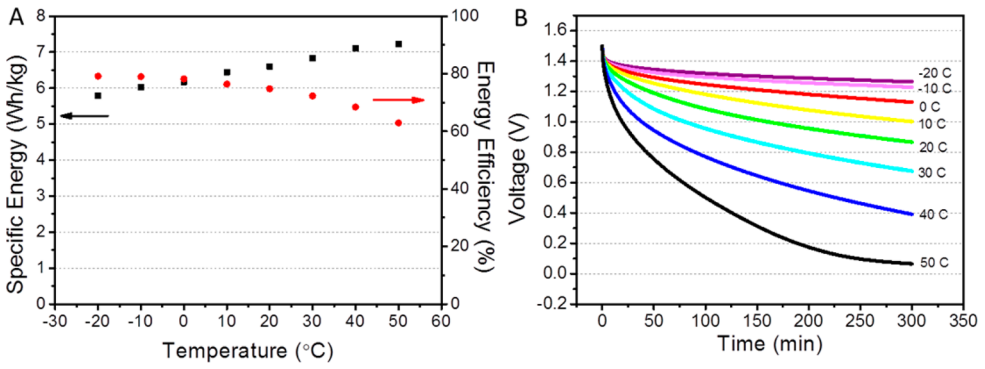

Figure 6. (A) Specific energy and round-trip energy efficiency at different temperatures. (B) Self-discharge for 300 min at different temperatures.

DOI: 10.1021/acsami.5b04677
ACS Appl. Mater. Interfaces 2015, 7, 19978−19985

■ ASSOCIATED CONTENT

Supporting Information

The Supporting Information is available free of charge on the ACS Publications website at DOI: 10.1021/acsami.5b04677.

BET results, optimal concentration determination, Raman spectra, and electrochemical comparison between KI in neutral solution and basic solution (PDF)

■ AUTHOR INFORMATION

Corresponding Author

*E-mail: david.ji@oregonstate.edu.

Author Contributions

⊥X.W. and R.S.C. contributed equally.

Notes

The authors declare no competing financial interest.

■ ACKNOWLEDGMENTS

This work is supported by Advanced Research Projects Agency Energy (ARPA-E), Department of Energy of the United States, Award number: DE-AR0000344 (control number 0670-3724). We acknowledge Mr. Jeff Morre and Dr. Liping Yang for mass spectrometry measurements. We thank Professor May Nyman and Mr. Harrison Neal for their help on Raman spectroscopy.

■ REFERENCES

(1) Kuperman, A.; Aharon, I. Battery-Ultracapacitor Hybrids for Pulsed Current Loads: A Review. *Renewable Sustainable Energy Rev.* **2011**, *15*, 981−992.

(2) Yoda, S.; Ishihara, K. The Advent of Battery-Based Societies and the Global Environment in the 21st Century. *J. Power Sources* **1999**, *81*, 162−169.

(3) Kotz, R.; Carlen, M. Principles and Applications of Electrochemical Capacitors. *Electrochim. Acta* **2000**, *45*, 2483−2498.

(4) Zhang, Y.; Feng, H.; Wu, X. B.; Wang, L. Z.; Zhang, A. Q.; Xia, T. C.; Dong, H. C.; Li, X. F.; Zhang, L. S. Progress of Electrochemical Capacitor Electrode Materials: A Review. *Int. J. Hydrogen Energy* **2009**, *34*, 4889−4899.

(5) Frackowiak, E.; Khomenko, V.; Jurewicz, K.; Lota, K.; Beguin, F. Supercapacitors Based on Conducting Polymers/Nanotubes Composites. *J. Power Sources* **2006**, *153*, 413−418.

(6) Lee, S. W.; Chen, S. O.; Sheng, W. C.; Yabuuchi, N.; Kim, Y. T.; Mitani, T.; Vescovo, E.; Shao-Horn, Y. Roles of Surface Steps on Pt Nanoparticles in Electro-Oxidation of Carbon Monoxide and Methanol. *J. Am. Chem. Soc.* **2009**, *131*, 15669−15677.

(7) Wang, X. F.; Raju, V.; Luo, W.; Wang, B.; Stickle, W. F.; Ji, X. L. Ambient Hydrolysis Deposition of TiO_2 in Nanoporous Carbon and the Converted Tin-Carbon Capacitive Electrode. *J. Mater. Chem. A* **2014**, *2*, 2901−2905.

(8) Hantel, M. M.; Kaspar, T.; Nesper, R.; Wokaun, A.; Kotz, R. Partially Reduced Graphite Oxide for Supercapacitor Electrodes: Effect of Graphene Layer Spacing and Huge Specific Capacitance. *Electrochem. Commun.* **2011**, *13*, 90−92.

(9) Futaba, D. N.; Hata, K.; Yamada, T.; Hiraoka, T.; Hayamizu, Y.; Kakudate, Y.; Tanaike, O.; Hatori, H.; Yumura, M.; Iijima, S. Shape-Engineerable and Highly Densely Packed Single-Walled Carbon Nanotubes and Their Application as Super-Capacitor Electrodes. *Nat. Mater.* **2006**, *5*, 987−994.

(10) Liu, C. G.; Yu, Z. N.; Neff, D.; Zhamu, A.; Jang, B. Z. Graphene-Based Supercapacitor with an Ultrahigh Energy Density. *Nano Lett.* **2010**, *10*, 4863−4868.

(11) Gogotsi, Y.; Nikitin, A.; Ye, H. H.; Zhou, W.; Fischer, J. E.; Yi, B.; Foley, H. C.; Barsoum, M. W. Nanoporous Carbide-Derived Carbon with Tunable Pore Size. *Nat. Mater.* **2003**, *2*, 591−594.

(12) Zhu, Y. W.; Murali, S.; Stoller, M. D.; Ganesh, K. J.; Cai, W. W.; Ferreira, P. J.; Pirkle, A.; Wallace, R. M.; Cychosz, K. A.; Thommes, M.; Su, D.; Stach, E. A.; Ruoff, R. S. Carbon-Based Supercapacitors Produced by Activation of Graphene. *Science* **2011**, *332*, 1537−1541.

(13) Wang, G. P.; Zhang, L.; Zhang, J. J. A Review of Electrode Materials for Electrochemical Supercapacitors. *Chem. Soc. Rev.* **2012**, *41*, 797−828.

(14) Zhang, L. L.; Zhao, X. S. Carbon-Based Materials as Supercapacitor Electrodes. *Chem. Soc. Rev.* **2009**, *38*, 2520−2531.

(15) Lee, S. W.; Kim, B. S.; Chen, S.; Shao-Horn, Y.; Hammond, P. T. Layer-by-Layer Assembly of All Carbon Nanotube Ultrathin Films for Electrochemical Applications. *J. Am. Chem. Soc.* **2009**, *131*, 671−679.

(16) Jiang, D. E.; Wu, J. Z. Microscopic Insights into the Electrochemical Behavior of Nonaqueous Electrolytes in Electric Double-Layer Capacitors. *J. Phys. Chem. Lett.* **2013**, *4*, 1260−1267.

(17) Jiang, D. E.; Jin, Z. H.; Henderson, D.; Wu, J. Z. Solvent Effect on the Pore-Size Dependence of an Organic Electrolyte Supercapacitor. *J. Phys. Chem. Lett.* **2012**, *3*, 1727−1731.

(18) Augustyn, V.; Simon, P.; Dunn, B. Pseudocapacitive Oxide Materials for High-Rate Electrochemical Energy Storage. *Energy Environ. Sci.* **2014**, *7*, 1597−1614.

(19) Malinauskas, A.; Malinauskiene, J.; Ramanavicius, A. Conducting Polymer-Based Nanostructurized Materials: Electrochemical Aspects. *Nanotechnology* **2005**, *16*, R51−R62.

(20) Peng, C.; Jin, J.; Chen, G. Z. A Comparative Study on Electrochemical Co-Deposition and Capacitance of Composite Films of Conducting Polymers and Carbon Nanotubes. *Electrochim. Acta* **2007**, *53*, 525−537.

(21) Sugimoto, W.; Yokoshima, K.; Murakami, Y.; Takasu, Y. Charge Storage Mechanism of Nanostructured Anhydrous and Hydrous Ruthenium-Based Oxides. *Electrochim. Acta* **2006**, *52*, 1742−1748.

(22) Qu, L. B.; Zhao, Y. L.; Khan, A. M.; Han, C. H.; Hercule, K. M.; Yan, M. Y.; Liu, X. Y.; Chen, W.; Wang, D. D.; Cai, Z. Y.; Xu, W. W.; Zhao, K. N.; Zheng, X. L.; Mai, L. Q. Interwoven Three-Dimensional Architecture of Cobalt Oxide Nanobrush-Graphene@$Ni_xCO_{2x}(OH)_{6x}$ for High-Performance Supercapacitors. *Nano Lett.* **2015**, *15*, 2037−2044.

(23) Ahn, Y. R.; Song, M. Y.; Jo, S. M.; Park, C. R.; Kim, D. Y. Electrochemical Capacitors Based on Electrodeposited Ruthenium Oxide on Nanofibre Substrates. *Nanotechnology* **2006**, *17*, 2865−2869.

(24) Mastragostino, M.; Arbizzani, C.; Soavi, F. Polymer-Based Supercapacitors. *J. Power Sources* **2001**, *97*−*98*, 812−815.

(25) Jiang, J. H.; Kucernak, A. Electrochemical Supercapacitor Material Based on Manganese Oxide: Preparation and Characterization. *Electrochim. Acta* **2002**, *47*, 2381−2386.

(26) Nelson, P. A.; Owen, J. R. A High-Performance Supercapacitor/Battery Hybrid Incorporating Templated Mesoporous Electrodes. *J. Electrochem. Soc.* **2003**, *150*, A1313−A1317.

(27) Hibino, M.; Abe, K.; Mochizuki, M.; Miyayama, M. Amorphous Titanium Oxide Electrode for High-Rate Discharge and Charge. *J. Power Sources* **2004**, *126*, 139−143.

(28) Hu, C. C.; Huang, C. M.; Chang, K. H. Anodic Deposition of Porous Vanadium Oxide Network with High Power Characteristics for Pseudocapacitors. *J. Power Sources* **2008**, *185*, 1594−1597.

(29) Chen, P. C.; Shen, G. Z.; Shi, Y.; Chen, H. T.; Zhou, C. W. Preparation and Characterization of Flexible Asymmetric Supercapacitors Based on Transition-Metal-Oxide Nanowire/Single-Walled Carbon Nanotube Hybrid Thin-Film Electrodes. *ACS Nano* **2010**, *4*, 4403−4411.

(30) Brezesinski, T.; Wang, J.; Senter, R.; Brezesinski, K.; Dunn, B.; Tolbert, S. H. On the Correlation between Mechanical Flexibility, Nanoscale Structure, and Charge Storage in Periodic Mesoporous Ceo2 Thin Films. *ACS Nano* **2010**, *4*, 967−977.

(31) Roldan, S.; Blanco, C.; Granda, M.; Menendez, R.; Santamaria, R. Towards a Further Generation of High-Energy Carbon-Based Capacitors by Using Redox-Active Electrolytes. *Angew. Chem., Int. Ed.* **2011**, *50*, 1699−1701.

(32) Tomai, T.; Mitani, S.; Komatsu, D.; Kawaguchi, Y.; Honma, I. Metal-Free Aqueous Redox Capacitor Via Proton Rocking-Chair System in an Organic-Based Couple. *Sci. Rep.* **2014**, *4*, 3591.

(33) Mai, L. Q.; Minhas-Khan, A.; Tian, X. C.; Hercule, K. M.; Zhao, Y. L.; Lin, X.; Xu, X. Synergistic Interaction between Redox-Active Electrolyte and Binder-Free Functionalized Carbon for Ultrahigh Supercapacitor Performance. *Nat. Commun.* **2013**, *4*, 2923.
(34) Lota, G.; Frackowiak, E. Striking Capacitance of Carbon/Iodide Interface. *Electrochem. Commun.* **2009**, *11*, 87−90.
(35) Lota, G.; Fic, K.; Frackowiak, E. Alkali Metal Iodide/Carbon Interface as a Source of Pseudocapacitance. *Electrochem. Commun.* **2011**, *13*, 38−41.
(36) Senthilkumar, S. T.; Selvan, R. K.; Lee, Y. S.; Melo, J. S. Electric Double Layer Capacitor and Its Improved Specific Capacitance Using Redox Additive Electrolyte. *J. Mater. Chem. A* **2013**, *1*, 1086−1095.
(37) Yu, H. Y.; Wu, J. H.; Fan, L. Q.; Xu, K. Q.; Zhong, X.; Lin, Y. Z.; Lin, J. M. Improvement of the Performance for Quasi-Solid-State Supercapacitor by Using Pva-Koh-Ki Polymer Gel Electrolyte. *Electrochim. Acta* **2011**, *56*, 6881−6886.
(38) Wang, B.; Maciá-Agulló, J. A.; Prendiville, D. G.; Zheng, X.; Liu, D.; Zhang, Y.; Boettcher, S. W.; Ji, X.; Stucky, G. D. A Hybrid Redox-Supercapacitor System with Anionic Catholyte and Cationic Anolyte. *J. Electrochem. Soc.* **2014**, *161*, A1090−A1093.
(39) Fic, K.; Meller, M.; Frackowiak, E. Interfacial Redox Phenomena for Enhanced Aqueous Supercapacitors. *J. Electrochem. Soc.* **2015**, *162*, A5140−A5147.
(40) Simon, P.; Gogotsi, Y. Materials for Electrochemical Capacitors. *Nat. Mater.* **2008**, *7*, 845−854.
(41) Noked, M.; Soffer, A.; Aurbach, D. The Electrochemistry of Activated Carbonaceous Materials: Past, Present, and Future. *J. Solid State Electrochem.* **2011**, *15*, 1563−1578.
(42) Bard, A. J.; Fraulkner, L. R. *Electrochemical Methods: Fundamentals and Applications*, 2nd ed.; John Wiley & Sons, Inc.: New York, 2001.
(43) Katsounaros, I.; Cherevko, S.; Zeradjanin, A. R.; Mayrhofer, K. J. J. Oxygen Electrochemistry as a Cornerstone for Sustainable Energy Conversion. *Angew. Chem., Int. Ed.* **2014**, *53*, 102−121.
(44) Li, C.; White, C. Kinetics of Hypoiodite Decomposition. *J. Am. Chem. Soc.* **1943**, *65*, 335−339.
(45) Buxton, G. V.; Mulazzani, Q. G. On the Hydrolysis of Iodine in Alkaline Solution: A Radiation Chemical Study. *Radiat. Phys. Chem.* **2007**, *76*, 932−940.
(46) Wren, J. C.; Paquette, J.; Sunder, S.; Ford, B. L. Iodine Chemistry in the + 1 Oxidation-State 0.2. A Raman and Uv-Visible Spectroscopic Study of the Disproportionation of Hypoiodite in Basic Solutions. *Can. J. Chem.* **1986**, *64*, 2284−2296.
(47) Jurewicz, K.; Frackowiak, E.; Beguin, F. Towards the Mechanism of Electrochemical Hydrogen Storage in Nanostructured Carbon Materials. *Appl. Phys. A: Mater. Sci. Process.* **2004**, *78*, 981−987.
(48) Beguin, F.; Friebe, M.; Jurewicz, K.; Vix-Guterl, C.; Dentzer, J.; Frackowiak, E. State of Hydrogen Electrochemically Stored Using Nanoporous Carbons as Negative Electrode Materials in an Aqueous Medium. *Carbon* **2006**, *44*, 2392−2398.
(49) Raju, V.; Rains, J.; Gates, C.; Luo, W.; Wang, X. F.; Stickle, W. F.; Stucky, G. D.; Ji, X. L. Superior Cathode of Sodium-Ion Batteries: Orthorhombic V2o5 Nanoparticles Generated in Nanoporous Carbon by Ambient Hydrolysis Deposition. *Nano Lett.* **2014**, *14*, 4119−4124.
(50) Conway, B. E.; Pell, W. G.; Liu, T. C. Diagnostic Analyses for Mechanisms of Self-Discharge of Electrochemical Capacitors and Batteries. *J. Power Sources* **1997**, *65*, 53−59.
(51) Ricketts, B. W.; Ton-That, C. Self-Discharge of Carbon-Based Supercapacitors with Organic Electrolytes. *J. Power Sources* **2000**, *89*, 64−69.

DOI: 10.1021/acsami.5b04677
ACS Appl. Mater. Interfaces 2015, 7, 19978−19985